Resonant inelastic x-ray scattering probes the electron-phonon coupling in the spin liquid κ -(BEDT-TTF) 2 Cu 2 (CN) 3

V. Ilakovac, S. Carniato, P. Foury-Leylekian, S Tomic, J.-P Pouget, P Lazic, Yves Joly, K. Miyagawa, K. Kanoda, A. Nicolaou

Resonant inelastic x-ray scattering probes the electron-phonon coupling in the spin-liquid κ-(BEDT-TTF)$_2$Cu$_2$(CN)$_3$

V. Ilakovac,[1,2] S. Carniato,[1] P. Foury-Leylekian,[3] S. Tomić,[4] J.-P. Pouget,[3]
P. Lazić,[5] Y. Joly,[6] K. Miyagawa,[7] K. Kanoda,[7] and A. Nicolaou[8]

[1]*Sorbonne Universités, UPMC, Univ. Paris 6, CNRS UMR 7614, Laboratoire de Chimie Physique – Matière et Rayonnement, Paris, France*
[2]*Université de Cergy-Pontoise, F-95031 Cergy-Pontoise, France**
[3]*Laboratoire de Physique de Solides, CNRS UMR 8502, Univ. Paris Sud, Université Paris Saclay, Orsay, France*
[4]*Institut za fiziku, P.O.Box 304, HR-10001 Zagreb, Croatia*
[5]*Ruder Bošković Institute, Bijenička cesta 54, HR-10000 Zagreb, Croatia*
[6]*Institut Néel, 25 Avenue des Martyrs, Grenoble, France*
[7]*Department of Applied Physics, University of Tokyo, Tokyo 113-8656, Japan*
[8]*Synchrotron SOLEIL, L'Orme des Merisiers, Saint-Aubin, B.P. 48, F-91192 Gif-sur-Yvette, France*

(Dated: December 6, 2017)

Resonant inelastic x-ray scattering at the N K edge reveals clearly resolved harmonics of the anion plane vibrations in the κ-(BEDT-TTF)$_2$Cu$_2$(CN)$_3$ spin-liquid insulator. Tuning the incoming light energy at the K edge of two distinct N sites permits to excite different sets of phonon modes. Cyanide CN stretching mode is selected at the edge of the ordered N sites which are more strongly connected to the BEDT-TTF molecules, while positionally disordered N sites show multi-mode excitation. Combining measurements with calculations on an anion plane cluster permits to estimate the site-dependent electron-phonon coupling of the modes related to nitrogen excitation.

I. INTRODUCTION

Electron-phonon coupling (EPC) plays a fundamental role in many aspects of condensed matter physics. It governs the charge mobility and optical properties in metals and semiconductors, it drives the Peierls metal-insulator instability in charge density wave compounds, it gives rise to the conventional superconductivity[1], while its role in the unconventional superconductivity is under persisting debate. Among experimental techniques permitting to measure the EPC strength, like infrared (IR), Raman, angle resolved photoemission spectroscopy, inelastic neutron scattering, and more recently ultrafast transient response of the optical reflectivity[2], neither of them is at the same time element-selective, site-dependent and momentum resolved like resonant x-ray scattering (RIXS). Last decade improvement of the resolving power of the RIXS spectrometers, going up to E/ΔE of 2.5 10^4,[3] promotes it to an excellent technique for the direct measurement of the EPC strength with all these advantages.

Understanding how the lattice dynamics couples to charge and spin degrees of freedom in κ-(BEDT-TTF)$_2$Cu$_2$(CN)$_3$ (shortly k-ET-Cu) is of primary importance for its spin-liquid[4] and pressure-induced superconducting properties[5–7]. This charge-transfer salt is composed of two alternating building blocs, as shown in Fig. 1(a). One is the donor layer of triangular constellations of dimers of ET (BEDT-TTF, bisethylenedithiotetrathiafulvalene) molecules. The other is the anion plane, consisting of triangularly coordinated copper(I) ions linked by cyanide (CN) groups[5]. The two are connected via C-H-N hydrogen bond. Each dimer donates approximately one electron to the anion plane, creating a triangular lattice of holes with a spin-1/2. The absence of spin ordering despite an exchange coupling of J $\approx$ 250 K was explained by the total frustration of spins on this triangular lattice[4]. But more recent ab-initio calculations pointed to slightly anisotropic transfer integrals between dimers[8,9] which rose the question of the origin of the spin-liquid state. A possible explanation lies in an interaction between spins and charge dynamics[10,11], and spinon-phonon interaction, as pointed by the ultrasonic wave measurements[12]. Finally, the actual debate on the role of phonons in the Cooper pairing applies perfectly to its pressure induced unconventional superconductivity[13].

There are many evidences of the strong dynamical and/or statical disorder in k-ET-Cu. An inherent disorder is present already in the conventional P2$_1$/c structure as one third of the anion plane CN groups lies on an inversion point and is thus orientationally disordered (see Fig. 1(b)). Moreover, ET-ethylene endgroups can take different conformations relative to the rest of the molecule, similarly to other (ET)$_2$X compounds[14,15]. Ethylene hydrogens form stronger H-bonding with nitrogens in ordered polymeric chains (N$_C$), compared to disordered bridging sites (N$_B$). A subtle interaction between electrons and lattice vibrations is observed in conducting and dielectric properties. DC conductivity shows an insulating behavior, described by nearest-neighbor hopping at ambient temperature, variable-range hopping below $\approx$ 130 K, while below 50 K, Hall measurements indicate a complete freezing of charge carriers[16,17]. Although there are no electric dipoles associated with the ET dimers[18], the fingerprints of relaxor ferroelectricity have been established by dielectric spectroscopy below 60 K[16,19].

In this work, we focus on the anion plane dynamics as this part of the system controls the donor packing and

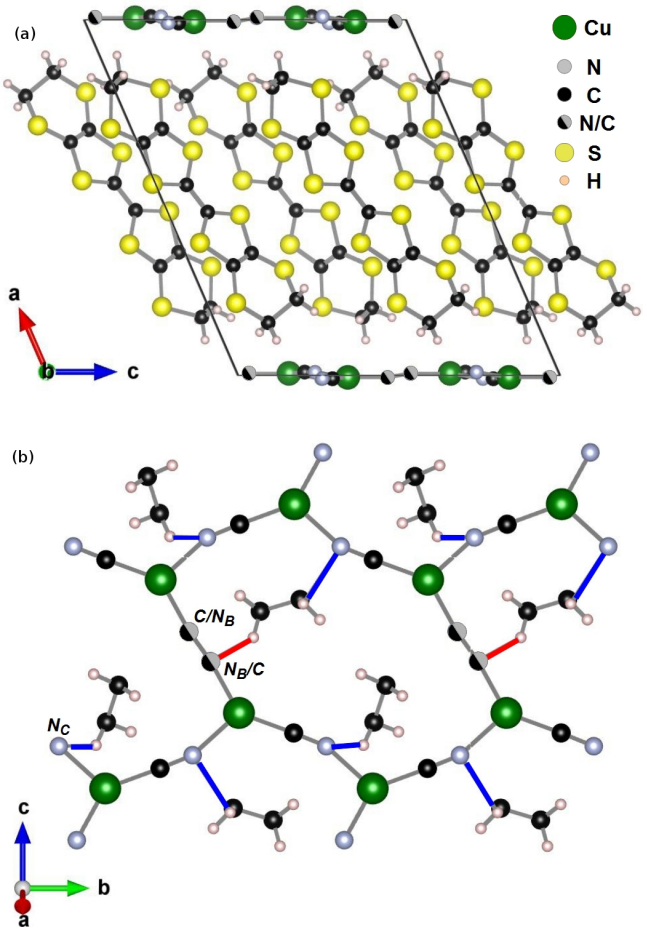

Figure 1. (a) k-ET-Cu structure seen along the b axis. (b) $Cu_2(CN)_3$ anion plane with Cu-CN_C-Cu polymeric chains and bridging, orientationally disordered, CN_B groups. Blue lines indicate HN_C bonds (2.72-2.79 Å) and red lines HN_B bonds (2.80 Å) connecting to ethylene endgroups of ET-molecules just below.

is an intrinsic source of disorder. We show that N K edge RIXS permits to switch-on two different dynamics related to nonequivalent nitrogen sites which are differently coupled to the ET molecular layer. One of these sites shows an essentially mono-mode excitation with five clearly resolved harmonics which show up in RIXS spectra. Despite the complexity of the system, our RIXS calculations, performed on an anion-plane cluster and including vibrational progression, describe well the experimental spectra and permit to determine the electron-phonon coupling of the selected phonon modes.

II. EXPERIMENTAL AND CALCULATION DETAILS

High quality single crystal sample of k-ET-Cu was grown by the electro-crystallization route[5,6]. N K edge ($\approx$ 400 eV) RIXS measurements were acquired at the SEXTANTS beamline (SOLEIL)[20,21] with an overall energy resolution of 115 meV. Near Edge X-ray Absorption Spectroscopy (NEXAFS) measurements were performed in the total electron yield mode with the beamline resolution set to 80 meV. Data were recorded in grazing incidence geometry (inset of Fig. 3), with the incoming photon polarization (ε) almost perpendicular to the anion layer $\angle(\varepsilon,\, a^*) = 20°$, or $\varepsilon \perp a^*$, where $a*$ stays for the reciprocal lattice vector perpendicular to the (b,c) plane. The orientation of the b and c axis with respect to the scattering plane was not determined. The sample was measured as introduced in a temperature range from 300 K to 25 K. NEXAFS calculations were performed by the Finite Difference Method Near Edge Structure (FDMNES) code[22,23] using coordinates of the conventional $P2_1/c$ structure[5]. RIXS calculations were performed on a five-cyanide cluster cut from the anion plane, $Cu_2(CN)_5H_4$. Its four peripheral cyanides were ended by hydrogen atoms in order to insure the chemical stability, while the central cyanide nitrogen was core-excited. Frequencies of the normal modes and the geometry optimization in the initial and the intermediate state of the RIXS process were calculated by DFT using the GAMESS(US) program[24]. For the quasi-elastic part of the spectra, the calculation of Franck-Condon amplitudes was performed by the method using the frequencies of the initial and the final state, and taking into account the deformation of the cluster from the initial to the intermediate state[25]. For the inelastic part of the spectra, the linear-coupling method was applied, where the initial and the intermediate state potentials are supposed to be harmonic, and of the same frequency.

III. NEXAFS SPECTRA REVEAL TWO DISTINCT NITROGEN SITES

Low temperature N K edge NEXAFS spectrum of the single crystal of k-ET-Cu is shown in Fig. 2. It has a prominent structure at the photon energy of hν = 399.8 eV and a low energy shoulder at about hν = 398.4 eV. In order to identify these two features, we performed calculation using the FDMNES code, for the two types of N sites (N_B, N_C) and for two orientations of the incident light polarization, parallel and perpendicular to a^*. The shape of N_B and N_C spectra is very different because the local environment of these two nonequivalent sites is not the same. For the same reason they also present a relative core level shift, higher for N_C compared to N_B. Indeed, the cation-ET-molecular layer imposes constraints to the anion plane, resulting in an elongation of the bridging Cu-CN_B-Cu and a compression and bending of the chain Cu-CN_C-Cu links (see Tab.I). The negative shift of the N_B feature of $\Delta E \approx 2.5$ eV compared to the main N_C structure is however overestimated compared to the experimental value of $\approx$ 1.5 eV. The reason for this discrepancy is the description of the orientational disorder of bridging CN_B cyanide groups in the conven-

	CN	CuN	CuC	CuCu	∠CuNC	∠CuCN
crystal						
Chain	1.130	2.026	1.872	4.933	158.9	177.3
Bridge	1.188	1.895	1.895	4.962	169.4	169.4
cluster						
initial state	1.156	1.928	1.931	5.013	176.2	178.8
excited state	1.195	1.991	1.845	5.026	176.1	178.9

Table I. Anion layer interatomic distances (in Å) and angles (in °) in the conventional crystal $P2_1/c$ structure[5]. They are compared to equivalent distances/angles in the cluster $Cu_2(CN)_5H_4$ used for RIXS calculation, in its initial and excited state.

tional $P2_1/c$ structure[5]. In this structure, CN_B groups are centered at inversion points. The CN_B distance is determined as the distance between statistical positions of C/N_B and N_B/C atoms, and is unnaturally increased. Moreover, the symmetry imposes equal Cu-C and Cu-N_B distances for a cyanide CN_B. On the other hand, in the case of chain Cu-CN_C-Cu links, the carbon is closer to its copper-neighbor and that the CN_C distance is shorter.

Further, the linear dichroïsm of the k-ET-Cu NEXAFS is surprisingly negligible, i.e. there is almost no polarization dependence when comparing spectra with $\angle(\varepsilon,a^*) = 20°$ and $\varepsilon \perp a*$ ($\varepsilon \parallel$ to (b,c) plane), as shown in Fig. 2. Though, NEXAFS spectra of a similar system, planar nitrile molecules, show two prominent white lines, corresponding to excitations to $\pi^*_\perp$ and $\pi^*_\parallel$ states, signs $\perp$ and $\parallel$ meaning relative to the molecular plane. Their relative shift of about 1 eV is explained by a conjugation-interaction inside the linear arrangement of C=C and C≡N bonds[27–30]. Linear C=C-C≡N geometry and a strictly planar system are therefore two conditions for a splitting of $\pi^*_\perp$ and $\pi^*_\parallel$ which are nominally degenerate. In FDMNES calculations of k-ET-Cu spectrum, N_C spectra projected to the $\pi^*_\perp$ and $\pi^*_\parallel$ states, $\perp$ and $\parallel$ meaning relative to the anion plane, are separated by only 0.5 eV. The conjugation effect is here decreased already by the 30° deviation from the linear arrangement of the Cu-CN_C-Cu bonds. The residual disagreement between the experiment and the FDMNES calculations in terms of the polarization dependence can be explained by the DFT approach. It does not describe correctly the effect of hydrogen bonding between the anion layer nitrogen and ethylene endgroup hydrogen atom. Note that this effect should be stronger for N_C (H-N_C = 2.72-2.79 Å) compared to N_B (H-N_B = 2.80 Å).

We stress the fact that even if the match between the experimental and the calculated NEXAFS spectra is not perfect, comparing them permits us to identify the NEXAFS main peak as related to the N_C sites and the low energy shoulder to the N_B sites.

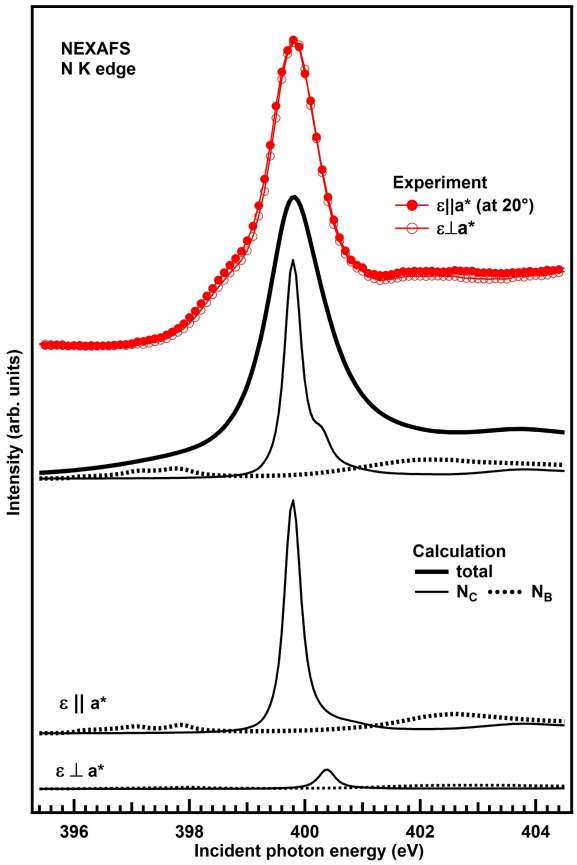

Figure 2. NEXAFS spectra (red circles) measured for $\angle(\varepsilon,a^*) = 20°$ and $\varepsilon \perp a*$ showing negligible polarization dependence. Calculated spectra (thick black line) is performed for $\angle(\varepsilon,a^*) = 20°$, and enlarged for taking into account the dynamics of the system. Contributions of N_C/N_B sites are shown without enlargement. The $\varepsilon \parallel a*$ and $\varepsilon \perp a*$ contributions of N_C/N_B sites is shown below.

IV. SITE-DEPENDENT LATTICE MOTION FINGERPRINTS IN THE QUASI-ELASTIC PART OF THE RIXS SPECTRA

Low temperature N K edge RIXS spectra are shown in Fig. 3. The experimental geometry is indicated in the inset. RIXS spectra were collected at photon energies indicated on the NEXAFS spectrum by the line of the same color. For incoming photon energies above $h\nu$ = 397.5 eV, the elastic peak develops an asymmetric tail, which transforms into a clear vibrational progression, concerning directly nitrogen sites of the anion CN groups. Recent detailed study of the k-ET-Cu lattice vibrations[26] reports that there are essentially three distinct families of modes affecting the CN groups. Their energy quanta will be designated by $\hbar\omega_n$, with n = 1,2,3. They are identified as CN stretching ($\hbar\omega_1$ = 260-265 meV), CN sliding between Cu atoms ($\hbar\omega_2$ = 60-65 meV), and low energy modes combining CN bending, stretching and twisting ($\hbar\omega_3$ = 8-50 meV), as presented in Tab. II. The

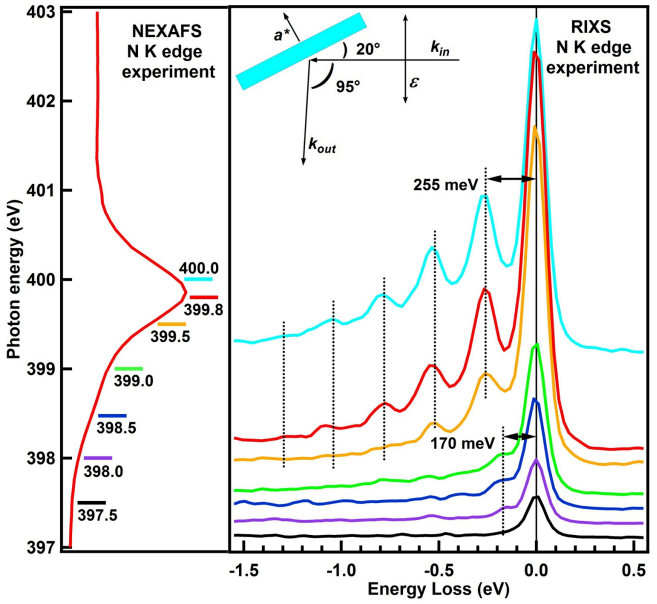

Figure 3. Low temperature NEXAFS (60 K, left) and RIXS (25 K, right) spectra, shifted for clarity. Inset shows the experimental geometry, with the polarization vector ε in the scattering plane.

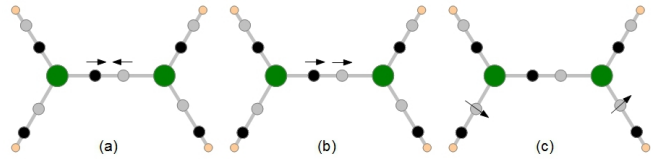

Figure 4. $Cu_2(CN)_5H_4$ cluster used for RIXS calculations and its most important normal modes: (a) CN stretching $\hbar\omega_1$, (b) CN sliding $\hbar\omega_2$, (c) CN bending $\hbar\omega_3$.

vibrational progression at hν = 399.5-400.0 eV shows distinct and perfectly resolved harmonics, separated by 255 meV, indicated by equidistant dotted lines. They are attributed to CN stretching motion ($\hbar\omega_1$). Below the NEXAFS maximum, in the range hν = 398-399 eV (NEXAFS shoulder), an energy loss of 170 meV is revealed (see Fig. 3(right)). Its energy does not correspond to any simple CN group movement and points rather to a multi-mode excitation.

In order to reproduce these experimental data we have performed RIXS calculations using the $Cu_2(CN)_5H_4$ cluster depicted in Fig. 4. It has been chosen as its interatomic distances and normal mode frequencies match well reported values in the k-ET-Cu crystal[5,26] (see Tab.I and Tab.II). However, it does not include effects of the ET-cation layer. The cluster has naturally linear Cu-CN-Cu arrangement characteristic of the C≡N bond, while in the real crystal, stronger H bonding of ethylene endgroups to the N_C- sites drags nitrogen in polymeric chains and deforms (bends) Cu-CN_C-Cu links (see Fig. 1 (b)). For Cu-CN_B-Cu bridging sites this deformation is much smaller.

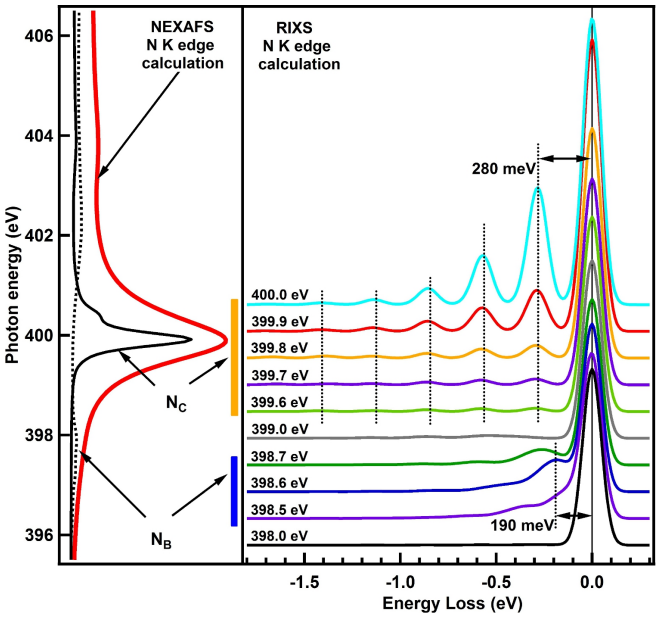

Figure 5. (left) NEXAFS calculation (red line) and N_C and N_B contributions. (right) RIXS calculation on a $Cu_2(CN)_5H_4$ anion plane cluster.

Mode	CN stretching	CN sliding	CN bending
n	1	2	3
crystal[26]	k-ET-Cu		
σ	2100-2140	508-515	195-225
$\hbar\omega$	260-265	63-64	24-28
cluster	$Cu_2(CN)_5H_4$	*calculations*	
σ_n (6%)	2258	510	200
$\hbar\omega_n$ (6%)	280	64	25
S_n (6%)	0.334	0.608	0.235
g_n (9%)	230	71	17
λ_n (35%)	0.076	0.032	0.004

Table II. Most important vibrational modes involving anion CN groups (see Fig. 4). Cluster calculation wave numbers (σ in cm^{-1}) and energy quanta ($\hbar\omega$ in meV) are compared to these in the crystal[26]. Corresponding values of Huang-Rhys parameters (S), gradients in dimensionless normal coordinates (g in meV) and dimensionless EPC (λ) are given with their relative errors in parentheses (%)[31].

Considering the grazing-incidence geometry explored in the experiment (see inset of Fig. 3), we considered that in the intermediate state the core electron is accommodated in the $\pi^*_\perp$ orbital system (perpendicular to the anion plane), while the initial and the final electronic states are the same. The calculated value of the 1s $\rightarrow$ $\pi^*_\perp$ transition of the $Cu_2(CN)_5H_4$ cluster is 398.6.0 eV, considered as the resonance of the N_B- sites. The reso-

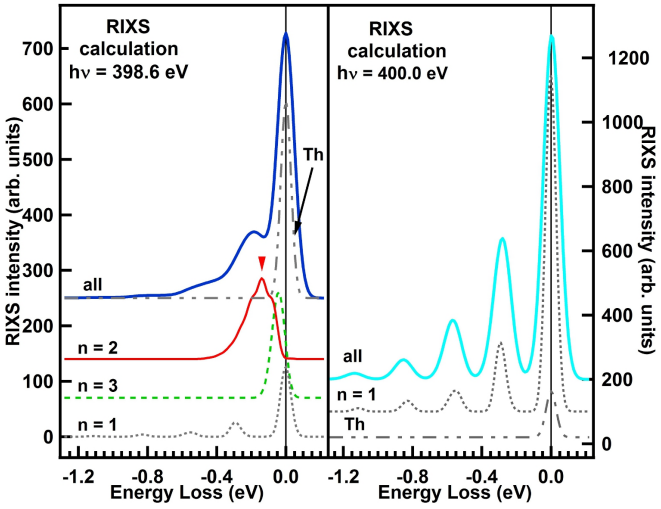

Figure 6. RIXS spectra calculated for $h\nu = 398.6$ eV (N_B sites, NEXAFS shoulder) and $h\nu = 400.0$ eV (N_C sites, NEXAFS main peak). Each spectrum is decomposed in its mono-mode contributions (n = 1-3) and the Thompson scattering (Th). For $h\nu = 398.6$ eV the second, most excited harmonics of the CN sliding motion (n = 2) is indicated by an arrow. Note that the "all" spectra include interference effects and experimental resolution broadening.

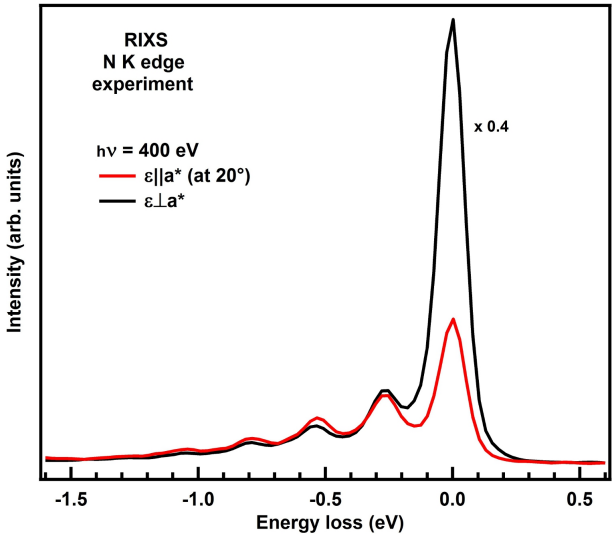

Figure 7. Experimental RIXS spectra measured at hν = 400 eV for two orientations of the incident electric field, $\angle(\varepsilon,a^*) = 20°$ and $\varepsilon \perp a*$. In order to better compare the two vibrational progressions, the intensity of the $\varepsilon \perp a*$ spectrum is multiplied by 0.4.

nance of the N_C- sites was set to 1.5 eV higher energy, corresponding to the energy difference between the two distinct behaviors observed in the RIXS experiment. In terms of phonon excitation, the final state differs strongly from the initial situation even if only few modes are relevant for the description of the quasi-elastic part of the spectra: CN stretching ($\hbar\omega_1$), CN sliding ($\hbar\omega_2$), and CN bending ($\hbar\omega_3$), depicted in Fig. 4.

In order to compare experimental data with calculations, calculated NEXAFS and RIXS spectra are shown in Fig. 5 in the same manner as the experimental results in Fig. 3. RIXS calculation shows that the resonant behavior of the vibrational progression calculated by this simple cluster model agrees well with the experiment.

When the RIXS calculation is performed for the photon energy $h\nu = 398.6$ eV, corresponding to the resonance of the N_B sites (NEXAFS shoulder), three normal modes are strongly excited. Fig. 6(left) shows the mono-mode contributions of the three modes (n = 1-3), elastic peak (Thomson scattering), and how they all interfere in the RIXS spectra ("all"). On the other hand, calculation with the photon energy set to $h\nu = 400$ eV (N_C sites, NEXAFS main peak), shown in Fig. 6(right) matches the experiment when solely CN stretching ($\hbar\omega_1$) is included. Clearly, real-crystal constraints in the curved Cu-CN_C-Cu conformation prevent strong excitation of any other motion related to the CN_C group. Strong excitation of any other mode would indeed completely destroy the CN stretching vibrational progression with distinct harmonics, similarly to the case of the N_B excited sites in the Fig. 6(left). Moreover, Cu-N and Cu-C distances in the real crystal are already close to these of the N K edge excited state cluster. Small excited state cluster deformation relative to the real crystal Cu-CN_C-Cu conformation explains the lack of vibrational modes besides highest energy CN stretching. Weak excitation of low-energy modes is however not excluded and should contribute to the tail of the elastic peak observed in the experiment. Finally, changing the polarization to $\varepsilon \perp a^*$ does not change the vibrational progression, only the intensity of the elastic peak (see Fig. 7).

Observed resonant modification of the vibrational progression in the quasi-elastic part of the N K edge RIXS spectra confirms that the NEXAFS main peak and the NEXAFS shoulder are related to two different nitrogen sites, N_C and N_B, respectively. With the help of RIXS calculations, we determine that the CN_C groups are restricted to almost mono-mode motion, while CN_B groups show up at least three strongly excited modes.

V. INELASTIC PART OF THE RIXS SPECTRA - CHARGE TRANSFER EXCITATIONS

Large energy-range RIXS spectra are shown in Fig. 8. They are presented in the emitted-energy scale in order to point to the almost non-Raman behavior of inelastic features A and B. Feature A appears at slightly lower incident photon energy (hν) and has almost constant intensity in a range of about 2 eV, while B resonates at hν = 399.8 eV, corresponding to the NEXAFS maximum. The emitted photon energy of their maximum is hν' $\approx$ 394.5 eV and $\approx$ 392.0 eV, respectively.

RIXS calculations are performed on the $Cu_2(CN)_5H_4$

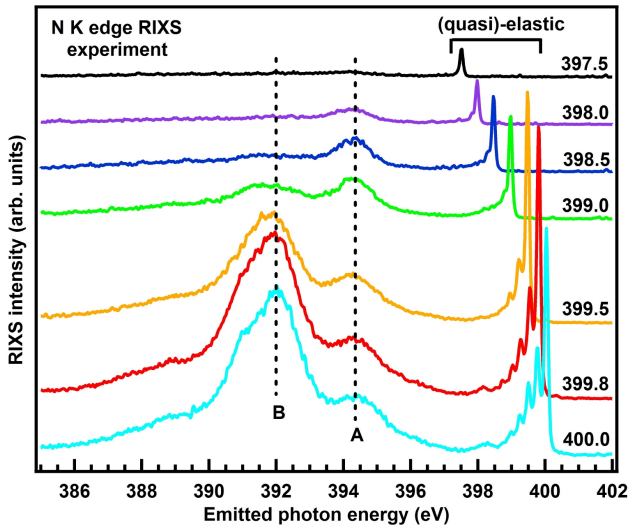

Figure 8. Emitted-energy scale (hν') RIXS spectra measured at 25 K. Corresponding incident photon energy (hν) is given at the right side of each spectra. Dashed line indicates the emitted energy of the structures A and B position at the NEXAFS maximum (hν = 399.8 eV).

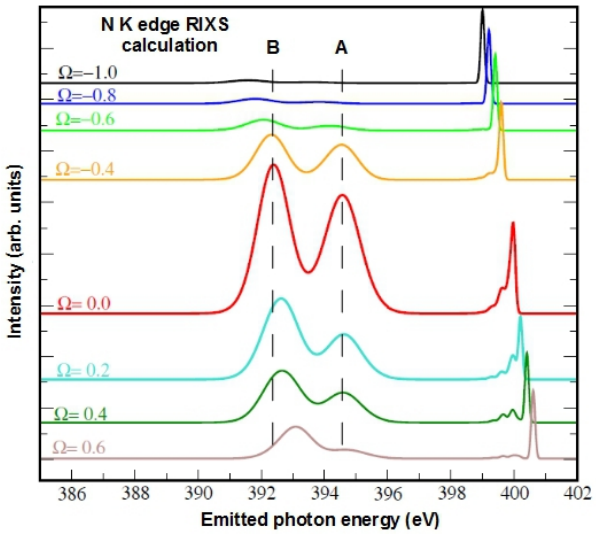

Figure 9. Calculation of the RIXS spectra including inelastic events. The detuning energy Ω (in eV), relative to the NEXAFS maximum, is indicated for each spectum. Dashed line indicates the position of the structures A and B for Ω = 0.

cluster (see Fig. 9), as for the quasi-elastic part. Structure A is identified as the excitation of an N 1s electron to the first non-occupied orbital ($\pi^*_\perp$) followed by the $\pi_\perp$, $\pi_\parallel$ → N 1s decay, giving rise to hν_{A1}, hν_{A2} emission, respectively, as schematized in Fig. 10(a). In terms of initial and final states, it is thus a signature of two transitions: $\pi_\perp \rightarrow \pi^*_\perp$ and $\pi_\parallel \rightarrow \pi^*_\perp$. The $\pi_\perp \rightarrow \pi^*_\perp$ transition is potentially related to the ET-cation → anion charge transfer, which is not described in the present anion-cluster calculations. The $\pi_\parallel \rightarrow \pi^*_\perp$ transition is a charge transfer from an orbital which is delocalized on three neighboring cyanides, to a $\pi^*_\perp$, which is localized mostly on the carbon atom of the central (excited) cyanide. The former is possibly related to the effective EPC including ET-molecular layer, while the latter is connected with the intra-anion-plane electron-phonon interaction. Similarly, the structure B with lower emitted energy (hν_B), can be described as the $\sigma \rightarrow \pi^*_\perp$ transition (see Fig. 10(b)).

As the $Cu_2(CN)_5H_4$ cluster is a system with discrete energy levels, features A and B are supposed to show Raman behavior, i.e. to shift in the emitted photon energy ($h\nu$') scale, in the same manner as the elastic peak. This shift is indeed present in the calculated spectra of Fig. 9 for incident photon energies ($h\nu$) away from the resonance. When the dynamics of the system is included via vibrational-progression calculations, their position remains constant when approaching the resonance, for hν ≈ 399.8 eV. Similar constant emitted-energy resonant behavior is observed in RIXS spectra of a very small system as the HCl molecule[32]. Thus, even for small systems, strong EPC induces non-Raman behavior in RIXS spectra.

In the inelastic part of the N K edge RIXS spectra three charge transfer excitations are identified: $\pi_\perp \rightarrow \pi^*_\perp$ and $\pi_\parallel \rightarrow \pi^*_\perp$ closer to the elastic peak, and $\sigma \rightarrow \pi^*_\perp$ with about 2 eV lower emitted energy. Cluster calculation including dynamics shows that their Raman behavior is suppressed at resonance.

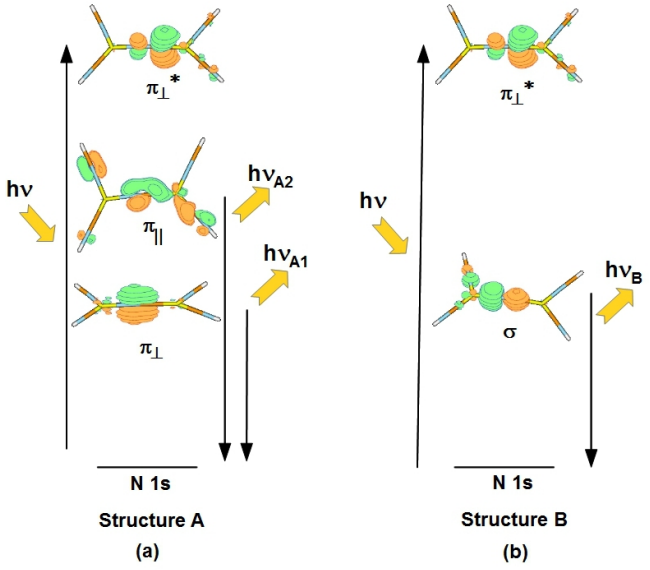

Figure 10. Inelastic RIXS processes giving rise to the structures A and B, with emitted photon energy, $h\nu' = h\nu_{A1}$, $h\nu_{A2}$ and $h\nu_B$. Lobes of the $\pi_\perp$, $\pi_\parallel$ and σ orbitals are presented in the initial state, the $\pi^*_\perp$ orbital in the excited state.

VI. EXTRACTING THE ELECTRON-PHONON COUPLING FROM THE RIXS SPECTRA

Theoretical work of Ament et al.[33] indicates how the EPC can be estimated from the envelope of the RIXS spectra vibrational progression. In the case of localized Einstein phonon modes, a simple expression is derived under ultra-short core-hole lifetime approximation ($\Gamma \gg \hbar\omega$). It relates EPC to the relative intensity of the first and the second harmonics, the core-hole lifetime broadening (Γ), and the phonon quantum ($\hbar\omega$). In this way, EPC of selected phonon modes was extracted from the Ti L edge RIXS spectra of titanates[34,35]. For the edge we are dealing with, this approximation is not valid, as both values of Γ reported in the literature, 93 meV[36] and 132 meV[36,37], are lower than $\hbar\omega_1 = 250$ meV.

Alternatively, the EPC of a selected mode n can be derived from our $Cu_2(CN)_5H_4$ cluster calculations. The demonstration will be performed using the linear-coupling model, where the potentials in the initial and the excited state, are supposed to be harmonic, of the same frequency, ω_n. The excited state is here a state with a core-hole and a supplementary electron in the valence band. Fig. 11 shows the two electronic-state potentials with corresponding vibrational wave functions. The phonon coupling to this electronic excitation is evaluated by the overlap of the initial state and the excited state wave functions. The excited state is shifted relatively to the initial state for a value of δq_n in normal coordinates. For small δq_n, the overlap of the initial and the excited state fundamental prevails, and the vibronic excitation is small. But, as δq_n increases, higher harmonics of the excited state have stronger overlap with the initial state wave function, leading to a stronger vibronic coupling. The Huang-Rhys (HR) parameter[38] evaluates overlaps of wave functions of the two harmonic potentials. It is calculated from the normal mode coordinate shift δq_n of the two potentials and their frequency:

$$S_n = \frac{\omega_n}{2\hbar}\delta q_n^2 \tag{1}$$

For the quasi-elastic part of the spectra, δq_n is calculated by taking into account the deformation of the cluster from the initial to the intermediate state[25]. Nevertheless, deriving of the EPC parameter is more evident when δq_n is calculated from the gradient of the excited state potential at $q_n = 0$ (green line in Fig. 11) as was done for the inelastic part of the spectra:

$$\delta q_n = \frac{1}{\omega_n^2}\left(\frac{\partial V_n^{exc}}{\partial q_n}\right)_{q_n=0} \tag{2}$$

Combining (1) and (2), S_n can be expressed as:

$$S_n = \frac{1}{2\hbar\omega_n^3}\left(\frac{\partial V_n^{exc}}{\partial q_n}\right)^2_{q_n=0} \tag{3}$$

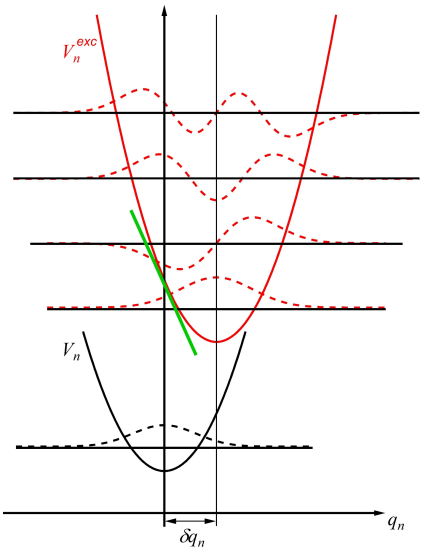

Figure 11. Initial state (black) and excited state (red line) potential and wave functions. Gradient of the excited state potential (V_n^{exc}) at $q_n = 0$ is indicated by a green line.

Using the transformation to dimensionless normal coordinates $q_n \to \sqrt{\hbar/\omega_n}Q_n$, S_n simplifies to:

$$S_n = \frac{1}{2}\frac{1}{(\hbar\omega_n)^2}\left(\frac{\partial V_n^{exc}}{\partial Q_n}\right)^2_{Q_n=0} \tag{4}$$

This permits to express the gradient of the excited potential in dimensionless normal coordinates directly in terms of the HR parameter:

$$g_n = \left(\frac{\partial V_n^{exc}}{\partial Q_n}\right)_{Q_n=0} = \hbar\omega_n\sqrt{2S_n} \tag{5}$$

In adiabatic EPC systems, where electron dynamics is much faster than phonon dynamics ($\omega_{el} \gg \omega_n$), the dimensionless EPC constant λ_n is defined, through BCS-type theory, as:

$$\lambda_n = \frac{g_n^2}{\hbar\omega_n}\chi(0) \tag{6}$$

where $\chi(0)$ is the electron-hole response function. Actually, the variation of atomic distances due to the excitation of the mode n induces a modulation of electronic transfer integrals inside the system under consideration, here the $Cu_2(CN)_5H_4$ cluster. This stimulates additional charge transfer and electron-hole pair creation.

For an insulating system with a localized or negligibly dispersing (Einstein) phonon, the electron-hole response function at $q_n = 0$ and ω_n=0 can be derived in the frame of the dimer-charge oscillation model[39,40]:

$$\chi(0) = \sum_{i,j} \frac{|\langle i|\hat{o}|j\rangle|^2}{\hbar\omega_{i,j}} \quad (7)$$

where the sum is performed over all possible electronic transition from the occupied state i to the unoccupied state j which are susceptible to be involved with the excitation of the phonon n. Supposing that the matrix elements of relevant processes are close to the unity, and all others are close to zero, $\chi(0)$ simplifies to:

$$\chi(0) = \frac{\mathcal{N}}{\hbar\omega_{CT}} \quad (8)$$

$\mathcal{N}$ being the number of electronic transitions with energy $\hbar\omega_{CT}$ which participate to the EPC.

A cyanide CN group phonon in k-ET-Cu modulates electronic transfer integrals inside the anion layer as well as between the anion and the cation layer. Two lowest energy electronic excitations in the cluster are chosen as charge transfer excitations which are related to the modulation of intra-layer and inter-layer electronic transfer integrals: the $\pi_\perp \rightarrow \pi^*_\perp$ and $\pi_\parallel \rightarrow \pi^*_\perp$. The value of $\mathcal{N}$ is thus 2, and the expression of λ_n becomes :

$$\lambda_a = \frac{2g_n^2}{(\hbar\omega_n)(\hbar\omega_{CT})} \quad (9)$$

where $\hbar\omega_{CT}$ corresponds to the minimal charge transfer excitation energy. It can be estimated from the calculation of the inelastic part of the spectra, in particular the energy of the $\pi_\parallel \rightarrow \pi^*_\perp$ and $\pi_\perp \rightarrow \pi^*_\perp$ excitations (structure A). The former is an in-plane charge transfer and the latter is possibly involved in the interaction with the ET-molecular layer. For the estimation of the $\hbar\omega_{CT}$ we took the value from the calculated spectra with detuning Ω = -0.4 eV, shown in Fig. 9. The value of $\hbar\omega_{CT}$ = 5 eV corresponds to the energy loss of the structure A, i.e. its position relative to the elastic peak, while its half-width-at-half-maximum is taken as the uncertainty $\Delta\hbar\omega_{CT}$ = 0.5 eV. Taking this value into account, for the CN stretching mode (hω_1 = 280 meV), with HR parameter S_1 = 0.334, and g_1 = 230 meV, we estimate the value of the dimensionless EPC parameter to be λ_1 = 0.076.

Tab. II shows the dimensionless EPC parameters of all the anion plane modes strongly excited by the N K edge RIXS process. They are individually lower than 0.08, but their total $\lambda_{anion} \approx 0.1$.

It is noteworthy that from IR and Raman measurements[40] the anion plane modes are considered to have negligible λ in the sister compound κ-(ET)$_2$Cu(SCN)$_2$. The same measurements reveal that the ET-molecular CC stretching mode is strongly coupled with λ_{CC} = 0.17. Similar measurements on β-(ET)$_2$I$_3$ estimate the total ET-molecular layer contribution to the EPC is $\lambda_{ET} \approx 0.4$[41]. Our estimation of the EPC in κ-(ET)$_2$Cu$_2$(CN)$_3$ shows that the coupling of the anion modes is certainly not negligible. Their contribution to the total λ is at least 20%.

Although the anion-donor coupling is not included in the present calculation, it is important to realize that the nitrogen displacement induces two types of indirect effects on the electronic structure of the ET layer. First, it tilts the H-bond, inducing (small) displacements of the ET molecule, which modulates the inter-ET transfer integrals. Second, it varies the H-bond distance and induces H bond polarization effect, which modulates inner σ electron density of the occupied levels of the ET-molecule[14]. This intra-molecular electron transfer, induces a modulation of the π-hole density on the core of the ET-molecules. A similar charge modulation process was previously invoked as a consequence of the establishment of H bonds accompanying the charge ordering transition in several family of ET salts[14,15].

Our data show that the EPC of N$_C$ sites, more strongly H-bonded to the ET-ethylene endgroups, involves almost solely the CN stretching motion. Besides, the EPC of the N$_B$ sites involves all cluster CN modes depicted in Fig. 4. This complex dynamics, together with the orientational disorder of CN$_B$ cyanides, creates a substantially disordered environment of each ET molecule, which is both statical and dynamical. The observation of the near-neighbor and variable range hopping mechanisms of conductivity[16,17] and the glassy behavior in dielectric spectroscopy[16] indicates that such a disorder is certainly relevant. We note that charge degrees of freedom play an important role in the physics of k-ET-Cu, meaning that one should go beyond the simple spin-liquid description originally considered[4], which takes into account only magnetic frustration between localized spins.

VII. CONCLUSION

We showed that the N K edge RIXS permits to clearly observe up to five lattice vibration harmonics of selected modes in κ-(BEDT-TTF)$_2$Cu$_2$(CN)$_3$ spin-liquid insulator. Tuning the incoming photon energy to the K edge of two non-equivalent N sites switches-on different sets of phonon modes. CN stretching mode is strongly excited at the edge of the ordered nitrogen sites which are more strongly connected to the BEDT-TTF molecules ($h\nu$ = 399.8 eV), while positionally disordered sites show multi-mode excitation ($h\nu$ = 398.4 eV). The difference in their resonant energy ($h\nu$) demonstrates that their environment alters the electronic state, while the complete change of their vibrational progression points to the degree of preventing the mechanical movement. RIXS spectra are reproduced by calculations on a cluster Cu$_2$(CN)$_5$H$_4$ cut from the anion plane and terminated by H atoms. They permit to estimate that the contribution of the anion-plane modes to the total dimensionless electron-phonon coupling parameter of the κ-(BEDT-TTF)$_2$Cu$_2$(CN)$_3$ compound is about 20%.

VIII. ACKNOWLEDGEMENT

S.T. acknowledges the support of the Croatian Science Foundation under the project IP-2013-11-1011. K. M. and K. K. acknowledge the support of Japan society for the Promotion of Science (JSPS) KAKENHI under Grant No. 25220709.

* vita.ilakovac-casses@upmc.fr

[1] F. Giustino, Rev. Mod. Phys. **89**, 015003 (2017)

[2] B. Mansart, D. Boschetto, A. Savoia, F. Rullier-Albenque, F. Bouquet, E. Papalazarou, A. Forget, D. Colson, A. Rousse, and M. Marsi, Phys. Rev. B **82**, 024513 (2010)

[3] L. Chaix, G. Ghiringhelli, Y. Y. Peng, M. Hashimoto, B. Moritz, K. Kummer, N. B. Brookes, Y. He, S. Chen, S. Ishida, Y. Yoshida, H. Eisaki, M. Salluzzo, L. Braicovich, Z.-X. Shen, T. P. Devereaux, and W.-S. Lee, Nature Physics, 12 June 2017, doi:10.1038/nphys4157

[4] Y. Shimizu, K. Miyagawa, K. Kanoda, M. Maesato, and G. Saito, Phys. Rev. Lett. **91**, 107001 (2003)

[5] U. Geiser, H. H. Wang, K. D. Carlson, J. M. Williams, H. A. Charlier Jr., J. E. Heindl, G. A. Yaconi, B. J. Love, M. W. Lathrop, J. E. Schirber, D. L. Overmyer, J. Ren, and M.-H. Whangbo, Inorg. Chem. **30**, 2586 (1991)

[6] T. Komatsu, N. Matsukawa, T. Inoue, and G. Saito, J. Phys. Soc. Jpn. **65**, 1340 (1996)

[7] Y. Kurosaki, Y. Shimizu, K. Miyagawa, K. Kanoda, and G. Saito, Phys. Rev. Lett. **95**, 177001 (2005)

[8] H. C. Kandpal, I. Opahle, Y.-Z. Zhang, H. O. Jeschke, and R. Valenti, Phys. Rev. Lett. **103**, 067004 (2009)

[9] H. O. Jeschke, M. de Souza, R. Valenti, R. S. Manna, M. Lang, and J. A. Schlueter, Phys. Rev. B **85**, 035125 (2012)

[10] C. Hotta, Phys. Rev. B **82**, 241104 (2010);

[11] S. Ishihara, J. Phys. Soc. Jpn **79**, 011010 (2010).

[12] M. Poirier, M. de Lafontaine, K. Miyagawa, K. Kanoda, Y. Shimizu, Phys. Rev. B **89**, 045138 (2014)

[13] F. Kagawa, K. Miyagawa, K. Kanoda, Nature letters **436**, 28 July 2005, doi:10.1038/nature03806

[14] P. Alemany, J.-P. Pouget, and E. Canadell, Phys. Rev. B **85**, 195118 (2012)

[15] P. Alemany, J.-P. Pouget, and E. Canadell, J. Phys.: Condens. Matter **27**, (2015) 465702

[16] M. Pinteric, M. Čulo, O. Milat, M. Basletić, B. Korin-Hamzić, E. Tafra, A. Hamzić, T. Ivek, T. Peterseim, K. Miyagawa, K. Kanoda, J. A. Schlueter, M. Dressel, and S. Tomić, Phys. Rev. B **90**, 195139 (2014)

[17] M. Čulo, E. Tafra, M. Basletić, S. Tomić, A. Hamzić, B. Korin-Hamzić, M. Dressel, J.A. Schlueter, Physica B **460**, 208 (2015).

[18] K. Sedlmeier, S. Elsässer, D. Neubauer, R. Beyer, D. Wu, T. Ivek, S. Tomić, J. A. Schlueter, and M. Dressel, Phys. Rev. B **86**, 245103 (2012)

[19] M. Abdel-Jawad, I. Terasaki, T. Sasaki, N. Yoneyama, N. Kobayashi, Y. Uesu, and C. Hotta, Phys. Rev. B **82**, 125119 (2010)

[20] M. Sacchi, N. Jaouen, H. Popescu, R. Gaudemer, J. M. Tonnerre, S. G. Chiuzbăian, C. F. Hague, A. Delmotte, J. M. Dubuisson, G. Cauchon, B. Lagarde and F. Polack, Journal of Physics: Conference Series **425**, (2013) 072018

[21] S. G. Chiuzbăian, C. F. Hague, A. Avila, R. Delaunay, N. Jaouen, M. Sacchi, F. Polack, M. Thomasset, B. Lagarde, A. Nicolaou, S. Brignolo, C. Baumier, J. Lüning, and J.-M. Mariot, Rev. Sc. Instr. **85**, 043108 (2014)

[22] O. Bunau and Y. Joly, J. Phys. : Condens. Matter **21**, 345501 (2009).

[23] S. A. Guda, A. A. Guda, M. A. Soldatov, K. A. Lomachenko, A. L. Bugaev, C. Lamberti, W. Gawelda, C. Bressler, G. Smolentsev, A. V. Soldatov, Y. Joly, J. Chem. Theory Comput. **11**, 4512-4521 (2015).

[24] M. W. Schmidt, K. K. Baldridge, J. A. Boatz, S. T. Elbert, M. S. Gordon, J. H. Jensen, S. Koseki, N. Matsunaga, K. A. Nguyen, S. Su, T. L. Windus, M. Dupuis, and J. A. Montgomery Jr., J. Comput. Chem. **14**, 1347 1993

[25] T. Darrah Thomas, L. J. Saethre, S. L. Sorensen and S. Svensson, J. Chem. Phys. 109, 1041 (1998)

[26] M. Dressel, P. Lazić, A. Pustogow, E. Zhukova, B. Gorshunov, J. A. Schlueter, O. Milat, B. Gumhalter, and S. Tomić, Phys. Rev. B **93**, 081201(R) (2016)

[27] S. Carniato, V. Ilakovac, J.-J. Gallet, E. Kukk, and Y. Luo, Phys. Rev. A **70**, 032510 (2004)

[28] S. Carniato, V. Ilakovac, J.-J. Gallet, E. Kukk, and Y. Luo, Phys. Rev. A **71**, 022511 (2005)

[29] V. Ilakovac, S. Carniato, J.-J. Gallet, E. Kukk, D. Horvatić, and A. Ilakovac, Phys. Rev. A **77**, 012516 (2008)

[30] V. Ilakovac, Y. Houari, S. Carniato, J.-J. Gallet, E. Kukk, D. Horvatić, Phys. Rev. A **85**, 062521 (2012)

[31] Standard error of DFT based calculations of vibrations is taken as the uncertainty of wave numbers $\Delta\sigma_n$ (and thus energy quanta $\Delta\hbar\omega_n$) of each mode. ΔS_n (Δg_n) is derived from the error of the relative shift of the excited and the initial state potential. $\Delta\lambda_n$ includes, besides Δg_n and $\Delta\hbar\omega_n$, $\Delta\hbar\omega_{CT}$ explained in the Sec.VI.

[32] M. Simon, L. Journel, R. Guillemin, W. C. Stolte, I. Minkov, F. Gel'mukhanov, P. Sałek, H. Ågren, S. Carniato, R. Taïeb, A. C. Hudson, and D. W. Lindle, Phys. Rev. A **73**, 020706 (2006)

[33] J. L. Ament, M. van Veenendaal, and J. van den Brink, E. Phys. Lett. **95**, 27008 (2011)

[34] S. Moser, S. Fatale, P. Krüger, H. Berger, P. Bugnon, A. Magrez, H. Niwa, J. Miyawaki, Y. Harada, and M. Grioni, Phys. Rev. Lett. **115**, 096404 (2015)

[35] S. Fatale, S. Moser, J. Miyawaki, Y. Harada, and M. Grioni, Phys. Rev. B **94**, 195131 (2016)

[36] J. L. Campbell, T. Papp, Atomic Data and Nuclear Data Tables 77, 1–56 (2001)

[37] M. Neeb, J.-E. Rubensson, M. Biermann and W. Eberhardt, J. Electron Spectrosc. 67, 261 (1994)

[38] K. Huang and A. Rhys, Proc. of Royal Soc. A, **204** 1078, 1950

[39] M. J. Rice, Solid State Commun., **31**, 93 (1979)

[40] R. D. McDonald, A.-K. Klehe, J. Singleton and W. Hayes, J. Phys.: Condens. Matter **15**, 5315 (2003)
[41] A. Girlando, M. Masino, G. Visentini, R. G. Della Valle, A. Brillante, and E. Venuti, Phys. Rev. B **62**, 14476 (2000)